Deploying Partially Cross-Linked Elastomers to Optimize Adhesion for Long-Term Surface Electromyography Electrodes

RESEARCH ARTICLE

ADVANCED MATERIALS INTERFACES Open Access

www.advmatinterfaces.de

Deploying Partially Cross-Linked Elastomers to Optimize Adhesion for Long-Term Surface Electromyography Electrodes

Yuqi Wang, Xi Wang, Leif Sandsjö, Xuqing Liu, and Li Guo**

Electrophysiological signals generated during daily activities are essential for monitoring and diagnosing various health conditions. Traditionally, Ag/AgCl electrodes with conductive gels have been used to capture these signals, recording them as electrocardiogram (ECG) and electromyogram (EMG). However, gelled electrodes glued to the skin presents challenges related to placement and are uncomfortable to wear for extended recordings. Recent studies have made significant advancements in dry electrodes for electrophysiological signals, mainly focusing on ECG applications with less emphasis on surface EMG (sEMG). To address this gap, this study introduces a novel set of skin-friendly electrodes made from a blend of conductive carbon black (CB) and partially cross-linked Ecoflex substrates. By varying the proportions of Ecoflex components A and B, a balance between adequate adhesion and electromechanical properties for good skin contact and long-term usabi is achieved, owing to the formation of silanol bonds. The CB-Ecoflex electrodes have been tested through over 50 wash cycles and 100 peel-offs, demonstrating strong durability and use resilience. Additionally, they maintain good recording conditions for 48 h and when sweat and oil are introduced on the skin. These electrodes consistently deliver reliable performance in 48-h continuous sEMG recordings, making them suitable for long-term applications.

1. Introduction

Electrophysiological signals generated during daily activities are essential for monitoring and diagnosing various health conditions. Conventionally, Ag/AgCl electrodes with conductive gels have been utilized in capturing these signals, recording them as electroencephalogram (EEG), electrocardiogram (ECG), electromyogram (EMG), and electrooculogram (EOG). However, the utilization of gels presents challenges, such as inconvenience and discomfort, making them unsuitable for extended monitoring. Recent studies have made significant advancements in the development of dry electrodes for electrophysiological signals, primarily focusing on ECG applications, with less emphasis on surface EMG (sEMG).[1] sEMG recordings are more susceptible to noise at the electrode-to-skin interface compared to ECG. This is due to the wider signal spectrum of 20–1000

Y. Wang, X. Liu
Shandong Laboratory of Yantai Advanced Materials and Green Manufacture
Yantai, Shandong 264006, China
E-mail: xqliu@amgm.ac.cn

Y. Wang, X. Wang
Department of Materials
School of Natural Sciences
the University of Manchester
Oxford Road, Manchester M13 9PL, UK

X. Wang, L. Guo
Swedish School of Textiles
University of Borås
Borås SE-501 90, Sweden
E-mail: li.guo@hb.se

L. Sandsjö
Department of Work Life and Social Welfare
University of Borås
Borås SE-501 90, Sweden

L. Sandsjö
Department of Industrial and Materials Science/Div of Design & Human Factors
Chalmers University of Technology
Göteborg SE-412 96, Sweden

X. Liu
Center of Advanced Lubrication and Seal Materials
State Key Laboratory of Solidification Processing
Northwestern Polytechnical University
Xi'an, Shaanxi 710072, P. R. China

The ORCID identification number(s) for the author(s) of this article can be found under https://doi.org/10.1002/admi.202400757

DOI: 10.1002/admi.202400757

Hz in sEMG (versus 0.05–100 Hz for ECG) and the potential skin deformation during muscle contraction.[2] Adequate electrode-to-skin adhesion is crucial to minimize electrode displacement and skin movement artifacts, ensuring accurate sEMG measurements.[3] Particularly, sEMG electrodes must be firmly attached to the skin under all conditions, including when skin sebum and sweat may be present during long-term recordings.[4] In contrast, excessive adhesion can cause user discomfort, including hair-pulling and skin damage during removal, and may also cause tensile deformation that influences the sensitivity, reusability, and durability of the electrode.[5]

The development of flexible dry surface electrodes has been focused on utilizing various materials and structural designs to enhance skin-electrode adhesion, flexibility, and electromechanical properties.[6] One approach involves incorporating elastomers, such as polydimethylsiloxane and polyurethane, as base material along with various conductive agents, including carbon black (CB), carbon nanotubes (CNT), graphene, metal nanowires, and intrinsically conductive polymers like PEDOT:PSS, as fillers.[4a,7] Among all the base materials considered, we found that Ecoflex has shown promise due to its flexibility, physical stability, and biocompatibility. In terms of conductive fillers, carbon black (CB) stands out as a cost-effective and non-toxic alternative to other fillers like CNT and graphene, and it is easy to process during manufacturing.[8] By combining Ecoflex and CB, researchers have created sensors and electrodes that exhibit strong durability, resilience, and high sensitivity. For instance, a study developed highly stretchable capacitive sensors using a printed carbon black/Ecoflex interdigital capacitor, demonstrating excellent stretchability and reliability for over 1000 cycles.[9] Another example is the development of gel-free ECG electrodes based on carbon black and Ecoflex, which showed high stretchability and conformability, making them suitable for long-term use without the need for conductive gels.[10] However, using Ecoflex for small-sized electrodes, such as those for sEMG, presents challenges, particularly in scenarios involving extensive movement. The smooth surface texture of Ecoflex can hinder the adhesion, impacting electrode performance.[11]

Addressing these challenges, we developed skin-friendly elastic electrodes from a blend of CB and partially cross-linked Ecoflex substrates (CB-Ecoflex) (**Figure 1a**). The CB-Ecoflex electrodes in this study were produced using a simple blending method to achieve the desired covalent cross-linking, forming an easy-bonding phase (Figure 1b). By varying the proportions of Ecoflex components A and B, deviating from the standard 1:1 ratio to 1:2 and 1:3 (so called partially cross-linked), and incorporating molecular chain steric hindrance, the CB-Ecoflex surfaces retain residual silanol groups' post-reaction with a silylating agent. This unique attribute influences water and oil contact angles (Figure 1b,e–h; Figures S1 and S2, Supporting Information), thereby improving skin adhesion. These electrodes ensure excellent skin contact (Figure 1c), can support weights up to 50 g (Figure 1d; Video S1, Supporting Information), and maintain adhesion even under challenging conditions, such as exposure to still and running water (Figure 1i,j and Videos S2 and S3, Supporting Information). They demonstrate robust and repeatable adhesion properties after 100 peeling cycles and over 50 wash cycles. The conductive network, facilitated by tunneling and interphase connections (Figure 1k), ensures adequate conductivity (9 kΩ/□ at 1000 Hz). As a proof-of-concept, these electrodes have shown high sensitivity in detecting subtle signals, positioning them as a promising option for advanced applications such as smart prosthetics.

2. Results and Discussion

2.1. Design Mechanism of CB-Ecoflex Materials

Through a comprehensive study involving various concentrations of CB (3%, 5%, 7%, 10%, 12%, 15%, and 18%) and Ecoflex proportions (1:1, 1:2, 1:3, and 2:3), we identified some higher-performing samples with more suitable ratios (10% and 12% CB with 1:2, 1:3, and 2:3 Ecoflex) for further experiments. As excessive CB can hinder cross-linking, insufficient CB results in high resistance. Additionally, different Ecoflex proportions resulted in different adhesive properties. Detailed test results are provided in this section and Supplementary Information. The fully and partially cross-linked phase compositions of the flexible adhesive electrode are shown in **Figure 2a,b**. Here, partial cross-linking indicates that not all polymer chains were fully cross-linked, resulting in incomplete network structures and free polymer chains from part B of Ecoflex. The lower cross-linking density and free polymers resulted in less rigid material with more terminal Si—H functional groups compared with the fully cross-linked Ecoflex. Furthermore, we analyzed the modulated cross-linking network structure through Fourier transform infrared spectroscopy (FTIR), skin impedance tests, and sEMG sections to understand their electrode-skin contact and conductivity properties.

2.2. Characterization of CB-Ecoflex Materials

As shown in (Figure 2c), the 10% CB:1:1 Ecoflex surface demonstrates a homogeneous distribution of CB particles, while wrinkles after 200% stretching (Figure 2d). To further clarify, Figure S3a (Supporting Information) presents the SEM image of 12% CB-Ecoflex, from which Figure 2c is a magnified view. Similarly, Figure S3b (Supporting Information) shows the SEM image of 12% CB-Ecoflex under 200% strain, and Figure 2d corresponds to its magnified region. Compared to the pristine Ecoflex surface (Figure S3c, Supporting Information), which appears smooth and featureless, the CB-Ecoflex surface reveals increased protrusions and emerging CB particles under strain. To assess the surface energy properties of the CB-Ecoflex samples, contact angles were measured (Figure 1e,f, g,h; Figures S1 and S2, Supporting Information). Notably, the sample containing 10% CB-blended partially cross-linked (1:3) Ecoflex exhibited the most favorable surface hydrophilic properties, with a water contact angle of 72° (Figure 1h). The contact angle (θ) is a crucial factor in determining substrate wetting, influenced by the surface energy (γs) of the substrate, surface tension (γl) of the liquid coating, and interfacial tension (γls) between them.[12] Notably, reduced contact angles indicate enhanced substrate wetting. Although hydrophilicity alone is not necessarily related to strong adhesion on the skin, this nature suggests the possibility of more hydrogen group presence in the material. This can promote stronger adhesion owing

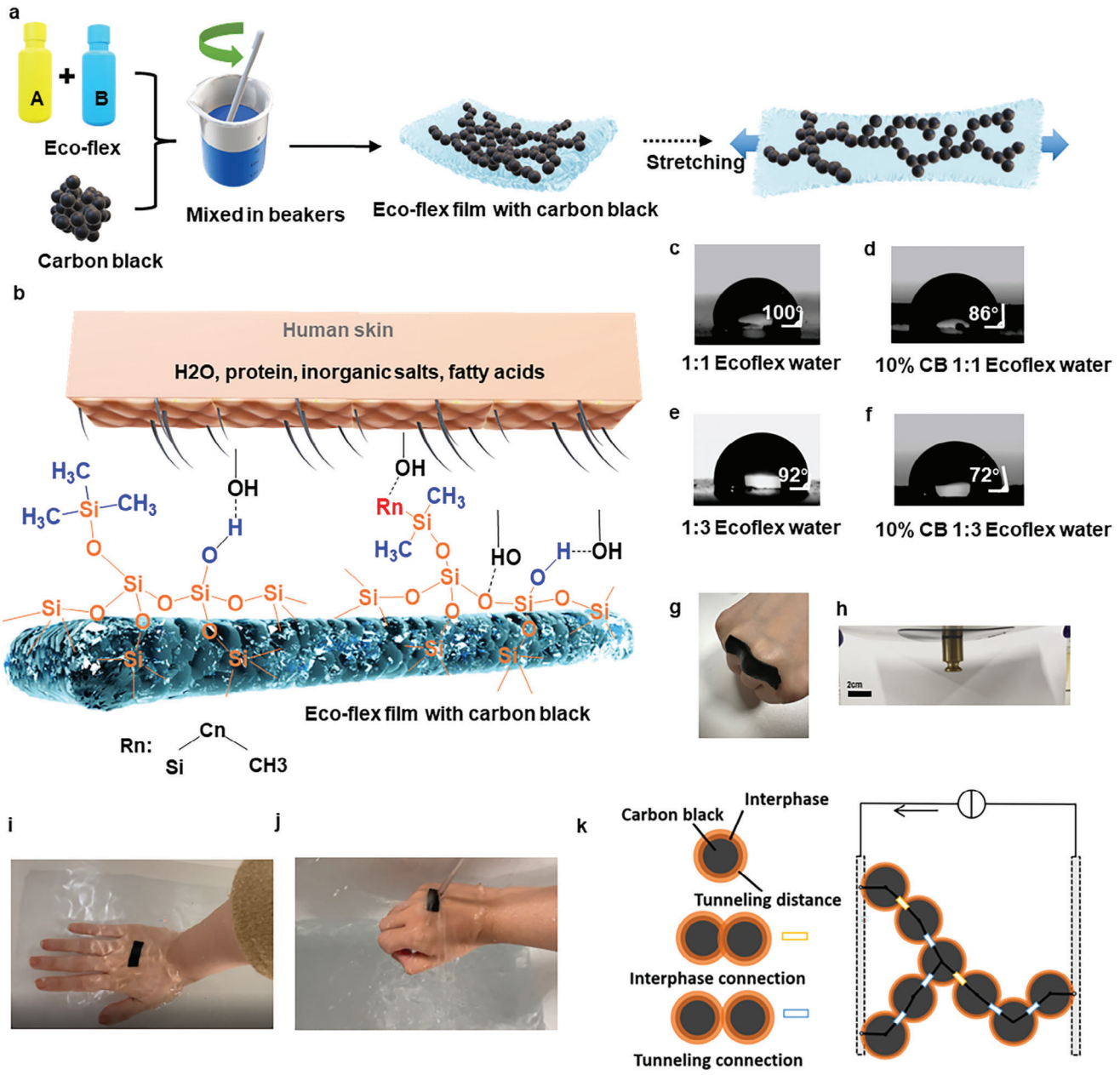

Figure 1. Elastic conductor design. a) Structural illustration: fabrication process, elastic networks of CB-Ecoflex conductors during stretching. b) Structural illustration: molecular structures, interaction between the skin and CB-Ecoflex conductor, through the interactions enabled by partially covalently cross-linked elastic networks. c–f) Digital image: water droplet on a fully cross-linked Ecoflex substrate (contact angle 100°) (c), CB-blended fully cross-linked ecoflex (contact angle 86°) (d), incompletely cross-linked Ecoflex (contact angle 92°) (e), and CB-blended incompletely cross-linked Ecoflex (contact angle 72°) (f). g) Image: CB-Ecoflex electrodes attached to the human skin demonstrating seamless contact. h) Excellent adhesion of CB-ecoflex: image showcasing the lifting of a weight of 50 g by stickiness, i,j) Digital image: stable interface connection between the skin and CB-Ecoflex electrode in water (i) and under running water (j). k) Mechanism illustration: conductive process of CB-Ecoflex conductors through the percolation theory and tunneling effect.

to the increased chemical interactions (hydrogen bonding) at the skin-electrode interface. By increasing the surface energy of the substrate, these interactions are further promoted, leading to improved and more reliable adhesion.[13]

Our analyses revealed that an excess of Part B in the CB-Ecoflex ratio resulted in numerous uncross-linked structures as linker groups, thereby enhancing adhesion to the skin (Figures S1 and S2, Supporting Information). This may be attributed to hydrogen bonding between the silanol groups and skin at their interfaces upon contact.[14] Moreover, the standard fully cross-linked Ecoflex conductor (with 1:1 ratio) exhibits a high contact angle(100°), and low peeling force (1.3 Nm^{-1}), which resulted in poor adhesion

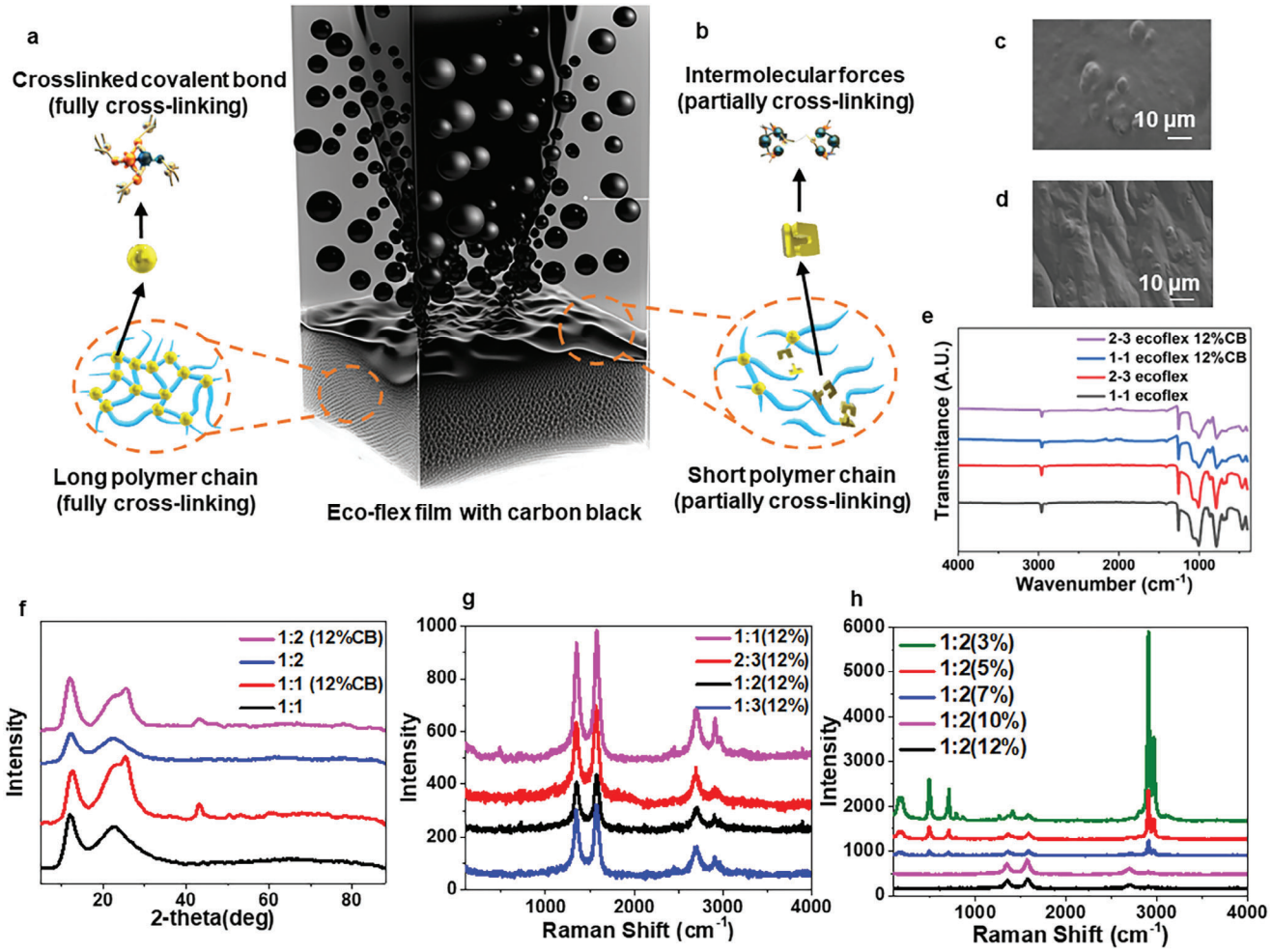

Figure 2. Mechanism of fully and partially cross-linked characterization. a) Structural illustration: CB distribution and the intermolecular force (free silicon hydroxyl group in gel) formation on the CB-Ecoflex conductor after fully cross-linked fabrication. b) Structural illustration: partially cross-linked CB-Ecoflex conductor after fabrication with covalent bonds. c, Scanning electron microscopy (SEM) images: surface morphology of 10 wt.% CB 1:1 Ecoflex before stretching. d) SEM images: surface morphology of 10 wt.% CB 1:1 Ecoflex after stretching under 25% tensile strain. e) FTIR analysis of the Ecoflex substrate with 12 wt.% CB 1:1 Ecoflex, 12 wt.% CB 1:2 Ecoflex, 1:1 Ecoflex, and 1:2 Ecoflex. f) XRD spectra of partially and fully cross-linked CB-Ecoflex including 12 wt.% CB 1:1 Ecoflex, 12 wt.% CB 1:2 Ecoflex, 1:1 Ecoflex, and 1:2 Ecoflex. g,h) Raman spectra of partially and fully cross-linked CB-Ecoflex (1:1, 2:3, 1:2, and 1:3) with 12 wt.% CB (g), and 1:2 Ecoflex with different CB concentrations (3%, 5%, 7%, 10%, and 12%) (h).

related with their inherent hydrophobic nature (Figure 1e,f; Figure S4, S8b, and S14, Supporting Information). By contrast, partial cross-linking with unoptimized ratios, such as 1:5, may lead to deformation issues, such as failure to fully recover the original shape after deformation.

Furthermore, we characterized the degree of cross-linking and structural integrity of Ecoflex before and after CB blending. In the FTIR analysis (Figure 2e; Figure S5, Supporting Information), distinct peaks were observed in the spectra of Ecoflex at 1255 and 1090 cm^{-1}. These peaks corresponded to the bending and rocking vibrations of Si—CH_3 and Si—O—Si stretching vibrations, respectively. These peaks are indicative of the polymer backbone and suggest the presence of cross-linking.[15] The presence of a peak at about 2958 cm^{-1} indicates the C—H stretching vibrations in the Ecoflex network, which is a characteristic feature of the polymer structure.[16] The absorption band at 910 cm^{-1} (Figure S5c, Supporting Information) was attributed to the stretching and bending vibration modes of Si—H bonds.[16] The part B sample exhibited a distinct absorption peak for the Si—H bonds, which were absent in part A. Meanwhile, compared with the 1:1 Ecoflex, the 1:3 Ecoflex exhibited more pronounced absorption. The Si—H bonds provided more opportunities for oxidation to form Si—OH, validated by the presence of -OH broad band absorptions at 3300–3700 cm^{-1} in the FTIR in Figure S5b (Supporting Information).[17] These weak characteristic peaks of -OH groups indicated the partial oxidation of Si—H to Si—OH on the exposed surface of Ecoflex. Additionally, after CB modification, the FTIR spectrum of the modified Ecoflex showed no significant alterations in the characteristic peaks associated with the cross-linking structure. The Si—O—Si stretching vibrations remained prominent, validating that the introduction of a moderate amount of CB did not cause significant destruction or disruption of the cross-linked network.

Moreover, the X-ray diffraction (XRD) patterns revealed variations in the degree of crystallinity based on the different ratios of Ecoflex components (Figure 2f).[18] All XRD patterns exhibited two primary Ecoflex refraction halos at ≈12° and 22°, indicating that the bulk properties of samples were not impacted by the characteristic amorphous microstructure and CB blending.[19] Upon incorporating 12% CB into 1:1 and 1:2 Ecoflex compositions, the XRD patterns demonstrated the presence of CB crystalline peaks at $2\theta = 26.6°$ (002) and $2\theta = 43.5°$ (10l), signifying successful blending.[20] The halo at 12° indicates non-crystalline regions owing to the random arrangement of the siloxane chains. Additionally, compared with pure 1:1 Ecoflex, the 1:2 Ecoflex compositions exhibited a lower intensity halo at ≈22°, indicating fewer crystalline regions with localized ordered structures.[21]

The incorporation of CB into the Ecoflex matrix was observed through Raman spectroscopy (Figure 2g,h; Figure S6, Supporting Information). The characteristic carbon-related peaks in the Raman spectra validate successful integration. Notable peaks at 487, 707, 2907, and 2963 cm^{-1} as well as D, G, and 2D bands at 1345, 1567, and 2691 cm^{-1}, respectively, affirm the combination between CB and Ecoflex.[18] Cross-linking typically involves the formation of Si—O—Si bridges. A noticeable decrease in the intensity of the cross-linking-related Raman peaks was identified as the CB-to-Ecoflex ratio increased, indicating that an increase in the CB concentration would influence the internal microstructure. At CB concentrations of 10% and 12%, the characteristic peaks of Ecoflex were not observed on the surface, indicating that the surface was predominantly covered by CB. This led to a significant decrease in surface resistance, with sample selection starting at 10%. The interaction between CB and Ecoflex presents an opportunity for further exploration during mechanical tests to uncover the complexities of their relationship.

2.3. Quality of CB-Ecoflex Electrode–Skin Interface

Skin adherence is an essential parameter for CB-Ecoflex electrodes, which is indicated by the peeling force.[22] The peeling force, assessed through a 180° peel test (**Figure 3a–c**), demonstrated a strong correlation with the Ecoflex ratio, particularly the concentration of the curing agent. Adhesion tests, similar to fracture experiments, can utilize Griffith's energy balance to comprehend the CB-Ecoflex adhesive behavior during peeling, utilizing principles of fracture mechanics.[23]

Enhanced adhesion (peeling force) of up to 4 N m^{-1} at a 1:3-part A: part B Ecoflex ratio correlated with decreased part A content, which was attributed to the molecular polarization strength and chemical structure variations. These partially cross-linked CB-Ecoflex exhibited high adhesiveness, preventing crack initiation at the interface owing to their high surface energy.

However, the addition of CB exceeding 12% decreased adhesion, as the fully cross-linked CB-Ecoflex interfaces promoted rapid crack propagation under stress intensity beyond a critical threshold, consistent with contact angle observations.[24] Excessive blending material (over 18% CB) could potentially compromise the mechanical properties of CB-Eecoflex. Notably, 10% CB-Ecoflex (1:2 and 1:3) and 12% CB- ecoflex (1:2 and 1:3) exhibited high adhesiveness with peeling forces of 2.2, 3.5, 2.0, and 3.8 N m^{-1}, respectively (Figure 3b,c). The viscosity average values corresponding to these formulations are presented in Figure S7a (Supporting Information), further illustrating the relationship between CB concentration, cross-linking ratios, and overall viscosity trends.

2.4. Electromechanical Performance

Achieving an optimal amount and uniform distribution of CB in the CB-Ecoflex electrode is crucial for recording sEMG signals. Low CB content (5% and 7%) results in surface resistance exceeding 100 kΩ at 0–800 kHz owing to isolated CB particles falling below the percolation threshold. This results in a lack of continuous conductive pathways (Figure 3e; Figure S8, Supporting Information).[25] Surpassing the percolation threshold, concentrations of 10%, 12%, 15%, and 18% established a complex interconnected CB particle network spanning the entire material, significantly enhancing CB-Ecoflex conductivity,[26] The absolute impedance values at 1000 Hz for different CB concentrations and cross-linking ratios are shown in Figure S7b (Supporting Information), further highlighting the impedance reduction as CB content increases beyond the percolation threshold. Consequently, these electrodes with a surface resistance below 80 kΩ at 0–800 kHz, and their good adhesive properties (Figure 3d,e; Figure S9, Supporting Information) demonstrated potential for sEMG recording.

We have also explored the relationship between strain and resistance, with a specific emphasis on evaluating the sensitivity of the samples using the parameter ΔR/R0. The initial resistance of the sample was denoted as R0, whereas the resistance after deformation was denoted as R. The difference between R and R0 was captured by ΔR. We accurately measured the sensitivity by utilizing a combination of a tensile machine and an impedance meter. Characterization of the resistance changes during mechanical stretching of the CB-Ecoflex electrodes revealed their compliance to various deformations, such as bending, twisting, and pulling (Figure 3f,g,h; Video S4, Supporting Information). The sensitivity of conductivity (ΔR/R0) of CB-Ecoflex increased from 1 to 4 during stretching owing to disruptions in the conductive network under external forces within an extensive percolation range (Figure 3i,j; Figure S8, Supporting Information).[27] The gauge factor (GF) values of the electrodes were determined using the formula (ΔR/R0)/strain ε.[28] For the 12wt.% CB-Ecoflex, the maximum elongation at break decreased to 420%, compared with the original Ecoflex 0010, which boasted an impressive strain limit of up to 600%.

When stretching the CB-Ecoflex with 10wt.% CB concentration to a maximum of 540% elongation, conductivity was maintained with a gradual decrease, whereas 15 wt.% CB-Ecoflex experienced a rapid decline in conductivity to two-thirds at its maximum tensile strain (Figure 3I; Figure S8, Supporting Information). These findings suggest that CB-Ecoflex with CB concentrations of 10wt.% and 1 2wt.% had low impedances and maintained their electromechanical properties. The mass ratios of 2:3 and 1:3 for CB-Ecoflex provided enhanced flexibility, demonstrating a trade-off between conductivity and mechanical flexibility.

Encased in an interphase layer, CBs are crucial in quantum tunneling and percolation, with the quantum interfacial effect influenced by the distance between the CB and inherent

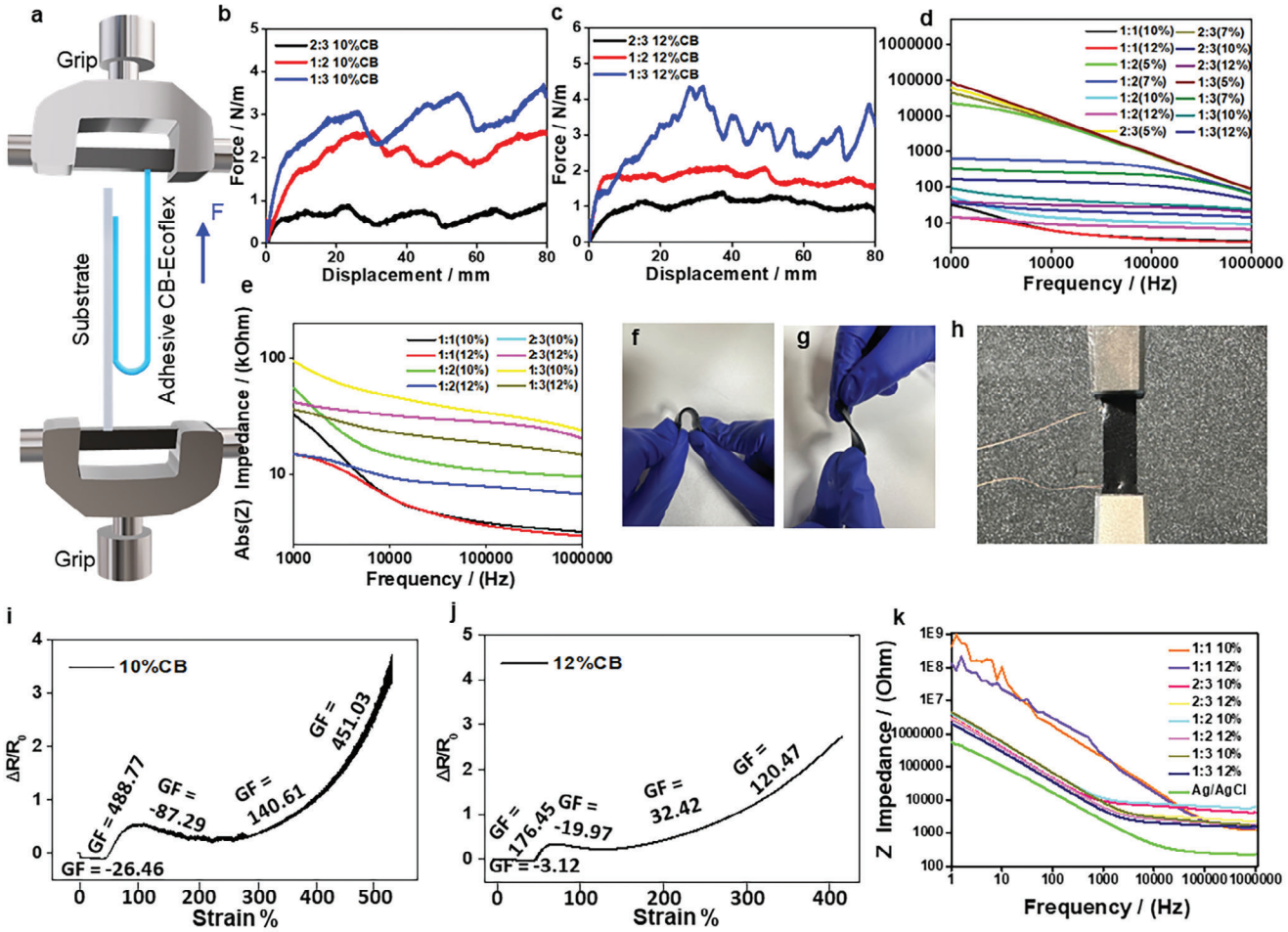

Figure 3. Interface adhesion and dynamic mechanical-electrical performance of the CB-Ecoflex electrode (part A). a) Illustration of 180° peeling test of the CB-Ecoflex electrode b) Measured peeling force of (2:3, 1:2, and 1:3) CB-ecoflex electrode with 10% CB content. c) Measured peeling force at CB-Ecoflex electrode ratios of 2:3, 1:2, and 1:3, with 12% CB content. d) Surface resistance of CB-Ecoflex with 5%, 7%, 10%, and 12% CB concentrations, comparing partially and fully cross-linked samples. e) A magnified view of the surface resistance data for 10% and 12% CB-Ecoflex, extracted from (d), to emphasize the detailed differences. f,g) Images of the CB-Ecoflex electrode under bending and twisting. h) Digital image of test resistance change in the CB-Ecoflex electrode during stretching. i,j) Resistance change (R/R0) of CB-Ecoflex (with different CB concentrations) under various tensile strains at a constant stretch speed (from left to right). k) Skin electrode impedance of the partially cross-linked CB-Ecoflex (with different CB concentrations), fully cross-linked CB-Ecoflex (with different CB concentrations), and commercial (Ag/AgCl) electrodes.

potential barrier of the polymer for maintaining stable conductivity during material elongation (Figure 1k). The electromechanical behavior of CB-Ecoflex, particularly at 10 and 12wt.% CB concentrations, demonstrated a nuanced four-step process as the strain increased, with each stage characterized by changes in the Gauge Factor as observed in the resistance/strain curves (Figure 3i,j; Figure S8, Supporting Information). i) Initial slippage and displacement (small bump): As the strain increased, the CB particles began to slip and displace, causing minor conductive pathway breakages. ii) Compression and electron tunneling (negative GF): During extension, the thickness decreased, densifying the CB particles under compression. In quantum mechanics, particles in close proximity, yet without direct contact, facilitate electron "tunneling" through the insulating barriers, thereby promoting conduction (Figure 1k).[29] Notably, as the interparticle distance decreased, the tunneling effect intensified.[30] iii) Extension and gap formation: Under relatively high strain, the extension and separation of the CB particles gradually transitioned into gaps within the material. iv) Significant separation and increased GF curves: A massive separation between the CB particles and larger hollow gaps in the matrix was observed under higher strain, resulting in a graph with increased GF curves. The aforementioned built-and-rebuilt CB-polymer matrix supported the conductive tunnel from the uniform dispersion of CB.[31]

Furthermore, our analysis revealed that the partially cross-linked CB-(2:3, 1:2, and 1:3) Ecoflex electrodes exhibited low electrode-skin impedances of 9 kΩ at 1000 Hz (Figure 3k; Figures S9 and S10, Supporting Information). This impedance was lower compared with that of similar electrodes reported previously (10 kΩ at 1000 Hz, PI-MNA(Au)).[32]

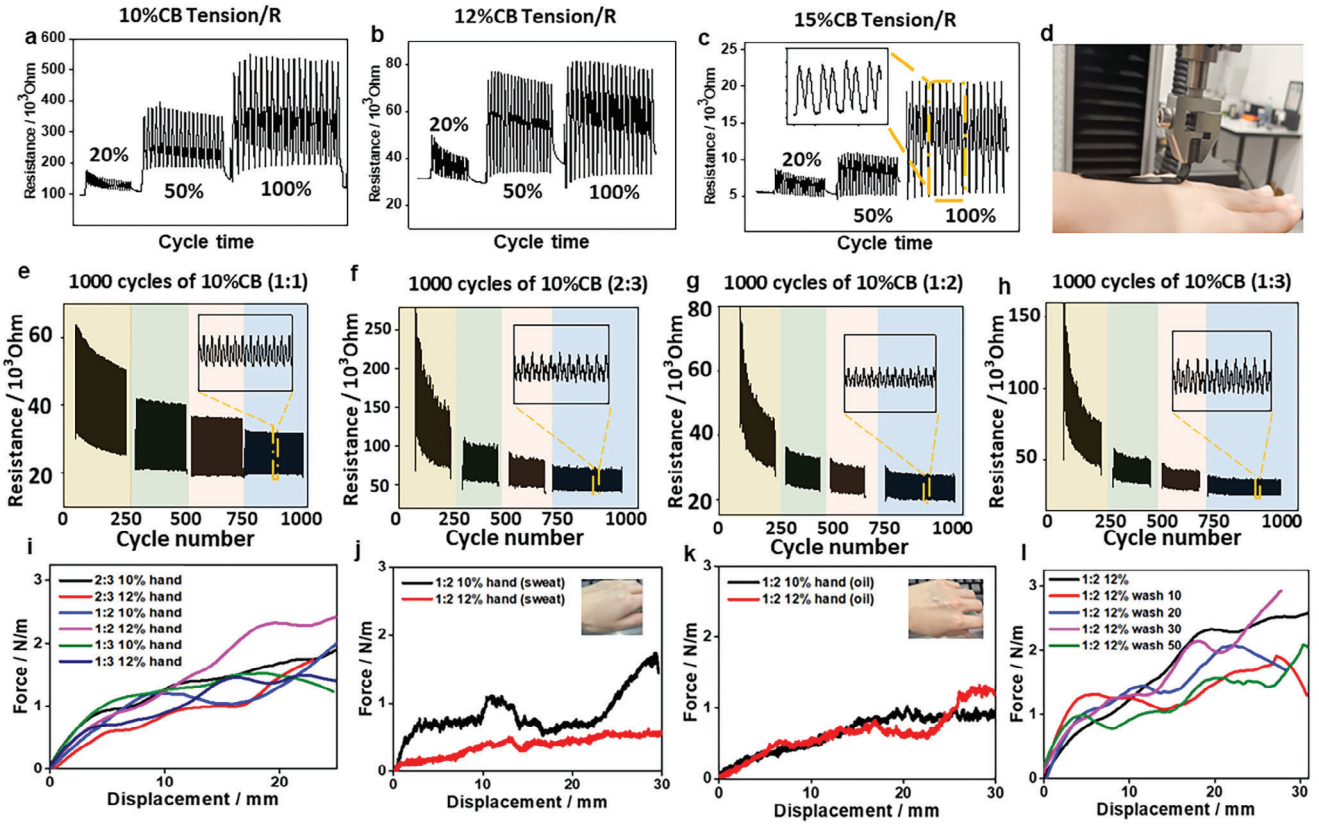

Figure 4. Interface adhesion and dynamic electromechanical performance of the CB-Eecoflex electrode (Part B). a–c) Resistance change in the Ecoflex substrates with 10 wt.% CB (a), 12 wt.% CB (b), and 15 wt.% CB (c) stretched under different elongations of 20%, 50%, and 100%, with a constant conductivity. d) Digital image indicating the peeling off of the CB-Ecoflex electrode from the skin. e–h) Durability of the partially and fully cross-linked CB-Ecoflex conductor (with 10% CB concentration) during 1000 stretch-release cycles under 25% tensile strain. i) Comparison of the curves of displacement versus peeling force when the (10% and 12%) CB – (2:3, 1:2, and 1:3) Ecoflex electrodes were on dry skin). j,k) Comparison of the curves of displacement versus peeling force when the CB-Ecoflex electrodes were on sweaty skin (j) and oily skin (k). l) Consistency of the peeling force of a (1:2) CB-Ecoflex electrode with a CB concentration of 12 wt.% after 50 cycles of washing in cyclic adhesion tests.

2.5. Durability Evaluation of Electromechanical and Adhesive Performance of the CB-Ecoflex

To investigate the durability performance of the electrodes, we examined the variations in relative resistances when subjected to tensile strains of 20%, 50%, and 100% (**Figure** 4a–c). Meanwhile, to evaluate long-term stability, the CB-Ecoflex electrodes underwent 1000 repeated stretch and release cycles at a speed of 30 mm min−1, with a maximum strain of ε = 25% (Figure 4e–h; Figure S11; Video S4, Supporting Information).

The reproducible electrical responses throughout fatigue testing, segmented and selectively displayed for clarity in Figure 4e–h, indicating minimal fluctuations of the 10% CB-Ecoflex and excellent stability and durability. The molecular structure of CB-Ecoflex is believed to adapt to mechanical strain during stretching, thereby maintaining its electrical conductivity and adhesive strength owing to its inherent elasticity. The resistance was relatively large at the first 200 cycles but became relatively stable after stretching and releasing. This is due to the continuous destruction and reconstruction of the CB conductive network during stretching/releasing cycles. Decreasing crosslinking density from 1:1 to 1:3 enhances viscosity, which promotes more frequent disruption and reformation of conductive pathways, leading to a more pronounced reduction in resistance.

Furthermore, we characterized the adhesion properties of these CB-Ecoflex electrodes under various skin conditions, including normal, sweaty, and oily conditions (Figure 4i,j,k). The peeling forces of samples with 10% and 12% CB-Ecoflex at a ratio of 1:2, reaching up to ≈2 N m^{-1} on human skin at 90° peeling angle, demonstrate the strength of adhesion (Figure 4d,I; Video S5, Supporting Information). However, adhesion was also influenced by factors, such as sweat and sebum, which can negatively impact adhesion through intermolecular forces (such as hydrogen bonding) and mechanical interlocking with the skin.[33]

Moreover, after undergoing 50 washing cycles, the electrodes with CB-Ecoflex ratio of 1:2 and CB concentration of 12 wt.% maintained adhesion, potentially enhancing skin-electrode contact by eliminating contaminants and exposing more silicon hydroxyl (Figure 4l).[34] Furthermore, a comprehensive analysis of the compression and rheological properties of CB-Ecoflex was conducted to assess its electrical performance under pressure (Figures S4a and S12, Supporting Information).

2.6. CB-Ecoflex Electrode Employed for sEMG

As a proof-of-concept study, CB-Ecoflex-based electrodes were utilized to record sEMG signals from the forearm of one of the authors (Figures S13 and S14; Videos S6–S11, Supporting Information). A pair of CB-Ecoflex electrodes (2 × 4 cm) was positioned on the extensor digitorum muscle on the posterior side of the forearm at an inter-electrode distance of 4 cm. Another pair of conventional Ag/AgCl electrodes (d = 1 cm) was placed on the same muscle, interspersed with the CB-Ecoflex electrodes so that both electrode pairs would pick up (almost) the same muscle activity from the forearm (**Figure** 5a). The interspersed electrode positions were also altered to enable comparable muscle activity recordings (Figure 5a). Data were obtained while extending the hand (wrist extension) to the maximum position (Figure 5f) for 3 s, followed by a 5-s rest.

Six distinct types of CB-Ecoflex-based electrodes, varying in mixture ratios (1:2, 1:3, and 2:3) and CB concentration (10% and 12%), were investigated considering the impact of interface adhesion and the conductivity, as previously discussed in Section 2.3. The electrodes were characterized and compared with standard Ag/AgCl electrodes in terms of signal quality. 'Electrode placement on different areas of the muscle can lead to variations in signal quality and amplitude due to differences in proximity to active muscle fibres or noise interference. In previous studies, specifically, both LIG/PPh and Ag/AgCl electrodes were positioned on the forearm in a crossed fashion, ensuring comparable placement for each type of electrode (**Figure** 6a in reference).[35] Therefore, in our study we 'co-located' electrodes during testing to minimize bias. We placed both the commercial electrode and our experimental electrode at the same location alternately, ensuring that both were positioned over the same muscle region during movements. This minimized variability caused by differing spatial sensitivities. Moreover, to eliminate any systematic placement bias, we exchanged the positions of the commercial electrodes and our experimental electrodes between tests. This ensured that no single position favored by one type of electrode.' As shown in Figure 5b, the mixture ratio was crucial in ensuring signal quality, with a 1:1 mixture ratio showing no detectable sEMG activity and a 1:3 ratio yielding results comparable to those of the Ag/AgCl electrodes. The poor adhesion of the electrode with a 1:1 mixture ratio is shown in Figure 5c. Conversely, as shown in Figure 5d, the electrode with a 1:3 mixture ratio securely adhered to the skin. These findings suggest a good skin-electrode adhesion improves the signal quality.

Signal-to-noise ratio (SNR) of the sEMG signals obtained using both types of electrodes in the same configuration is shown in Figure 5a. To eliminate the potential measurement bias associated with the electrode placement, we recorded the sEMG with an altered electrode position. The results indicated no significant difference in signal quality when both types of electrodes were placed on the same muscles. A visual representation of the detected signals and noise is shown in Figure 5e, with a detailed description of the methodology provided in Section 4. The SNR values for both the Ag/AgCl and CB-Ecoflex electrodes obtained during test contractions of the wrist are shown in Figure 5h. The Ag/AgCl electrodes exhibited similar SNR values, whereas the CB-Ecoflex electrodes exhibited lower SNR values with greater variability. Generally, the Ag/AgCl electrodes have higher SNR values compared with those of CB-Ecoflex electrodes, indicating better signal quality and reduced noise.

When comparing the two CB concentrations, 10% and 12% across all mixture ratio groups, no significant differences were observed. However, an analysis of the impacts of the mixture ratios showed a notable trend. Lower mixture ratios were associated with higher SNR values, suggesting improved performance. Notably, a mixture ratio of 1:3 yielded the most promising results, with SNR values of 31.9 dB and 29.6 dB in the 10% and 12% concentration groups, respectively. This suggests that a 1:3 mixture offers the optimal tradeoff between CB concentration and SNR performance.

As shown in Figure 5i, both Ag/AgCl and CB-Ecoflex electrodes maintained excellent signal quality even after 48 h of continuous use without being removed from the skin. Additionally, we examined the reusability of the electrodes by conducting sEMG quality tests for up to 100 removal and repositioning cycles. The results (Figure 5j) indicated a slight reduction in signal amplitude over repeated utilization. However, the signals generated when the hand was extended to the maximum position were easily distinguishable. These findings indicate that the electrodes exhibited promising reusability with no significant degradation in the detection of sEMG signals.

CB-Ecoflex electrodes were tested on sweaty skin (simulated by saline) and the skin was covered with a thick layer of oil-based cream to record sEMG activities. As shown in Figure 5k, the signal quality was satisfactory when the electrodes were placed on sweaty skin. However, when applied to skin covered in oil-based cream, no signals were detected. Subsequently, the oil-based cream was removed and the electrodes were washed. Signals were detected after only one wash; however, the signal quality was not enhanced with further washing as shown in Figure 5i, according to which the signal amplitude decreased after washing and further decreased after a rest period of two weeks under ambient room conditions. This reduction in the signal quality after washing suggests a potential permanent decline, warranting further investigation.

Another noteworthy observation was the presence of visible marks on the skin after the electrode removal. The marks from the CB-Ecoflex electrodes vanished completely, leaving no residual marks after 48 h, (Figure 5n, left). The subject reported no skin irritation or discomfort when wearing the CB-ecoflex electrodes, even during long durations. The ease of application was also an advantage, as the electrodes could be easily repositioned without losing adhesion, making them more user-friendly. In contrast, the marks from the Ag/AgCl electrodes persisted even after two weeks. It is difficult to remove due to its gel adhesive, frequently causing discomfort, including skin pulling and irritation, particularly for subjects with sensitive or hair-covered skin. This issue arose commonly post-removal. These finding suggests that CB-ecoflex electrodes, with higher biocompatibility and permeability, are more suitable for long-term monitoring compared with Ag/AgCl electrodes (which were limited to a 48-h testing period owing to laboratory constraints). However, the observed stability of the CB-ecoflex electrode suggests potential for extended use beyond the tested 48 h.

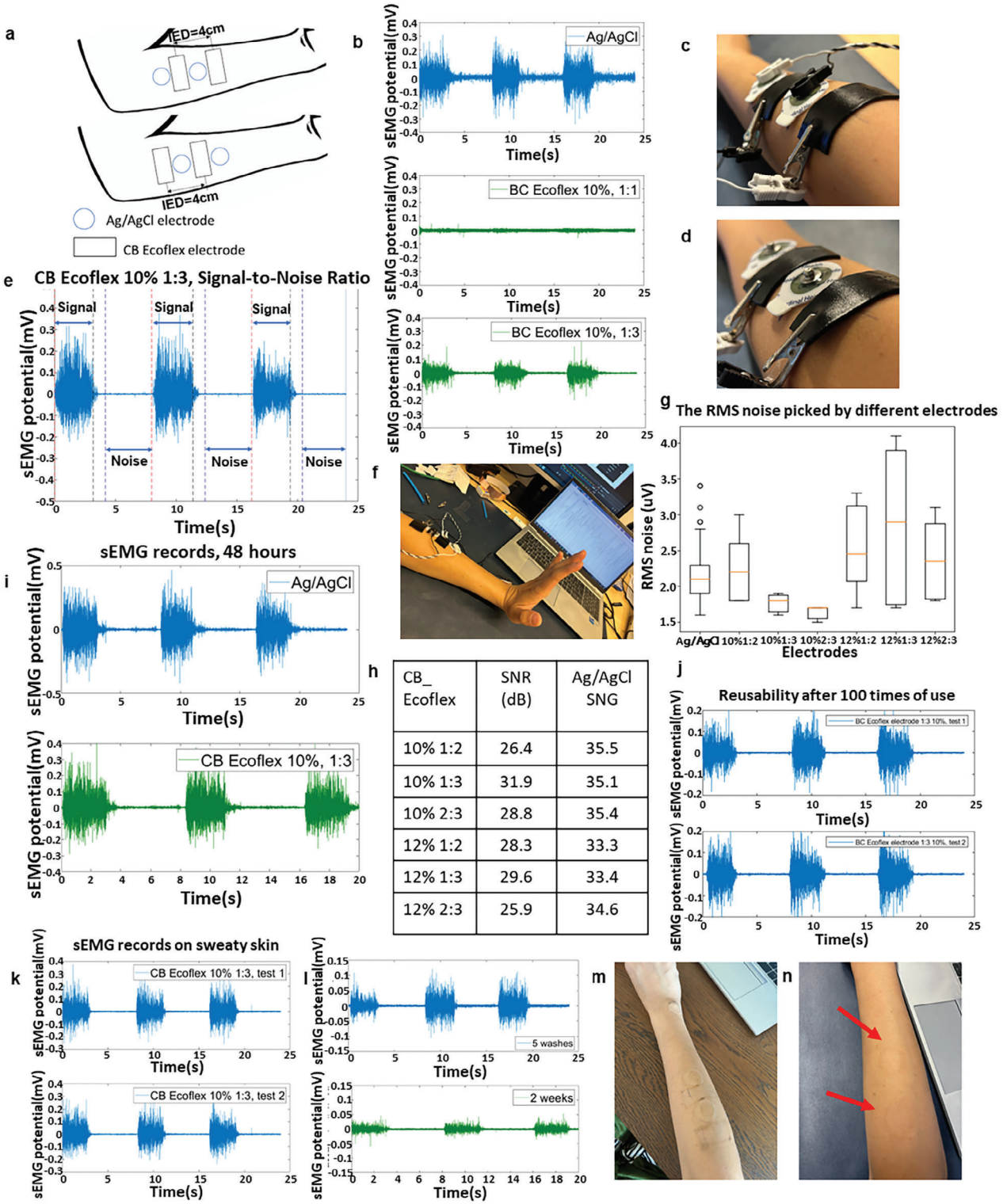

CB_ Ecoflex	SNR (dB)	Ag/AgCl SNG
10% 1:2	26.4	35.5
10% 1:3	31.9	35.1
10% 2:3	28.8	35.4
12% 1:2	28.3	33.3
12% 1:3	29.6	33.4
12% 2:3	25.9	34.6

Figure 5. Performance of CB-Ecoflex-based electrodes. a) pair of CB-Ecoflex electrodes staggered with a pair of Ag/AgCl electrodes on the posterior side of the forearm. b) sEMG recorded from CB-Ecoflex electrodes with 1:1 and 1:3 mixture ratios compared with the Ag/AgCl electrode. c) Electrodes placed on the forearm (mixture ratio 1:3). d) Electrodes placed on the forearm (mixture ratio 2:3). e) Recorded sEMG signals indicating signal and noise level. f) Hand extends to the maximum position, used for detecting SNR. g) RMS noise of the six types of CB-Ecoflex electrodes compared with an Ag/AgCl electrode. h) SNR of the six types of CB-Ecoflex electrodes on par with the Ag/AgCl electrode, movement recorded simultaneously. i) sEMG recorded after 48 h. j) sEMG recorded after 100 cycles. k) sEMG on a sweaty skin. l) sEMG recording after 5 washes and the application of oil-based cream on the skin and after 2 weeks. m) Photograph of the skin after removing the electrodes from the skin, after 48 h of recording. n) Photograph captured 2 weeks after removing the electrodes from the skin.

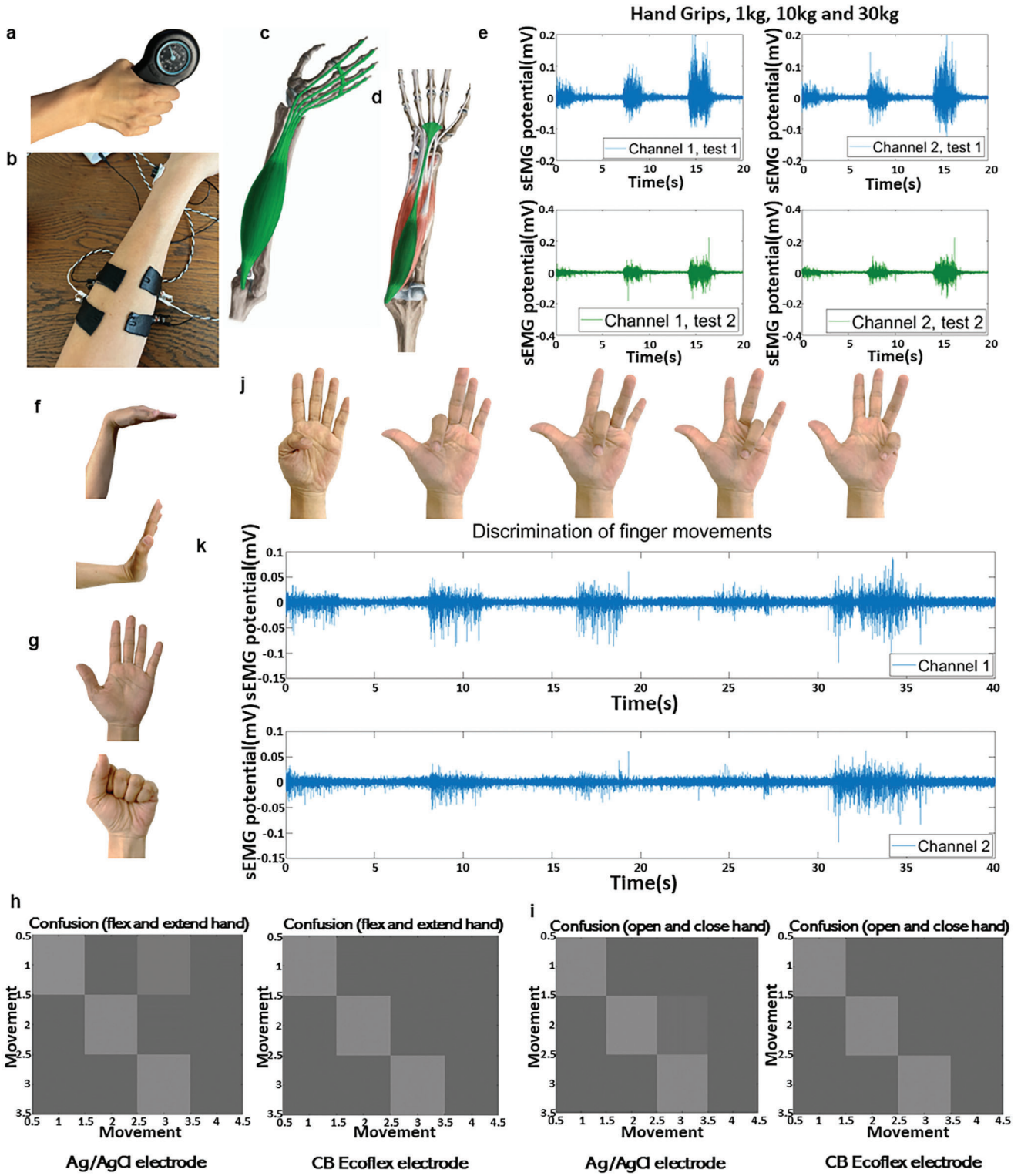

Figure 6. Potential utilization of CB-Ecoflex electrodes for prosthetic control and sEMG-based rehabilitation. a) Holding the hand grip. b) Placement of electrodes on the extensor digitorum and musculus palmaris logus. c) Extensor digitorum muscle[KENHUB]. d) Musculus palmaris longus muscle[KENHUB]. e) sEMG with grip forces of 1, 10, and 30 kg. f) Digital image of hand flexion and extension. g) Digital image of open and closed hands. h) Confusion matrix of hand flexion and extension, recorded from both Ag/AgCl and CB-Ecoflex electrodes. i) Confusion matrix of open and closed hands, recorded from both Ag/AgCl and CB-Ecoflex electrodes. j) Digital image of finger movements. k) sEMG of finger movements.

2.7. Potential Applications of CB-Ecoflex Electrodes

The potential application of CB-Ecoflex electrodes for prosthetic control and sEMG-based rehabilitation is promising. As dry electrodes, they eliminate the need for conductive gels or preparation, streamlining the electrode placement process. Additionally, their comfort and non-irritating nature enable long-term wear without discomfort or skin irritation. These electrodes provide reliable sEMG recordings with good signal quality and adhesion, even on sweaty skin. Moreover, the ability to reuse the electrodes multiple times without significant degradation in signal quality or performance enhances their cost-effectiveness and convenience, making them well-suited for applications requiring long-term and continuous monitoring or use. As a proof-of-concept study, we demonstrated the use of CB-Ecoflex electrodes in three cases.

CB-Ecoflex electrodes were used to monitor sEMG signals from the forearm under various gripping forces. In this study, two pairs of electrodes were positioned on the extensor muscles as shown in Figure 6c,d. The results demonstrated that when forces of 1, 10, and 20 kg were applied to the grip strength meter (Figure 6a), the CB-Ecoflex electrodes effectively demonstrated an increase in sEMG signals (Figure 6e).

Two pairs of the same electrodes were utilized for hand posture recognition, as shown in Figure 6b, on the extensor digitorum and musculus palmaris longus. Two pairs of movements were performed, "open hand" versus "closed hand" (Figure 6f) and "flex hand" versus "extend hand" (Figure 6g). These movements were considered as computational options as outlined in the Methodology Section 4.

Confusion matrices were generated to assess the performance of the classification algorithms for each movement pair. Two sets of confusion matrices were obtained based on recordings obtained using Ag/AgCl and CB-Ecoflex electrodes. Analysis of the confusion matrices (Figure 6h,i) indicates similar results for both movement pairs and electrode types. Both electrodes exhibited satisfactory performance in the given classification task, with any minor differences likely attributed to the complexity of the task rather than the electrode utilized.

Finger movements typically generate lower-amplitude EMG signals compared with hand movements, making it a more challenging test. In this study, two pairs of electrodes were positioned on the posterior (channel 1; Figure 6k) and anterior (channel 2, Figure 6k) sides of the forearm. Visual inspection revealed that different finger flexions resulted in different signals, showcasing the capability of CB-Ecoflex electrodes to discern myoelectric activity at a level suitable for prosthesis control.

3. Conclusion

This study explored a set of skin-adhesive and stretchable electrodes composed of CB blended with partially cross-linked Ecoflex. One of the key advantages of the CB-Ecoflex electrodes lies in their ability to maintain reliable sEMG signals without causing the discomfort associated with repeated removal. These electrodes exhibited a maximum peeling force of 4 N m^{-1} at a 1:3 part A to part B Ecoflex mixture ratio, high conductivity (skin-electrode interfacial impedance of 9 kΩ/□ at 1 kHz), a remarkable maximum elongation at break of 540.0%, and excellent signal quality even after 48 h of continuous use (without removal from skin). The electrodes were tested in sEMG applications, showcasing the possibility of repeatedly recording high-quality sEMG for 100 removal and repositioning cycles in daily life, while retaining adhesiveness and excellent skin compliance. This makes them an attractive alternative for applications where user comfort is a priority. By offering this balance between performance and comfort, these electrodes contribute to the development of more user-friendly wearable electronics, particularly for long-term monitoring applications. Moreover, the results from the hand gesture and finger movement discrimination tests suggest that CB-Ecoflex electrodes are as effective as Ag/AgCl electrodes for controlling prosthetic hands, holding promise for self-administered health monitoring, human-machine interaction, and rehabilitation. Future research will focus on the development of electrodes with enduring adhesion across diverse contexts, ensuring comfort, long-term utilization, and enhanced usability.

4. Experimental Section

Materials: Ecoflex (00–10) was purchased from Smooth-On Inc., and carbon black (CB, acetylene, 100% compressed, 99.9+% with S.A. 75 m^2 g^{-1} and bulk density of 170–230 g L^{-1}), from Alfa Aesar. All materials were utilized directly with no additional treatment.

Fabrication of Adhesive CB-Ecoflex Dry Electrode: CB-Ecoflex electrodes were prepared with different cross-linking ratios (1:1, 1:2, 1:3, and 2:3) and CB contents of 3 wt.%, 5 wt.%, 7 wt.%, 10 wt.%, 12 wt.%, 15 wt.%, and 18 wt.%. In the case of the 10 wt.% CB-1:2 Ecoflex electrode, 3 g of Ecoflex curing agent A and 6 g of Ecoflex base B with 1 g of CB were mixed. The weight percentages of Ecoflex and carbon black were adjusted to obtain electrodes with the desired properties. The mixture was then applied to the prepared model and degassed for 2 h before being cured overnight at room temperature.

Morphology and Structural Characterization of the Electrodes: The surface and sectional morphologies of the electrodes were examined through scanning electron microscopy (SEM, Zeiss Ultra 55, accelerating voltage 3 kV). X-ray diffraction (XRD, Phillips PANalytical X'Pert Pro X-ray diffractometer, scanning rate 0.02° step, 2θ range from 4° to 90° with a copper (Cu K α, $\lambda = 0.154$ nm) tube X-ray source) was utilized to investigate the crystalline structures within the samples. Fourier transform infrared spectroscopy (FTIR, Bruker Vertex 80) provided insights into the functional groups and chemical bonds present. Additionally, Raman spectroscopy (Renishaw RM1000 – 514 nm, laser spot size 1 µm) was employed to analyze the vibrational characteristics of the molecular structures. The hydrophilicity and lipophilicity of the dry electrodes were assessed using a DSA100 contact angle goniometer.

Evaluation of the Electromechanical Properties: The peeling force between the electrode and plastic substrates was measured using a tensile strength gauge. Compression and tensile tests were conducted on an INSTRON 4301 universal testing machine with a 500 N load cell and crosshead speed settings of 5 and 30 mm min^{-1}. Rheological properties were tested using a rheometer (Discovery HR-3 hybrid rheometer). The resistance of the electrodes was measured using the Keithley 2000 Series: 6½-Digit Multimeter with Scanning. The resistance was measured with the two probes of the instrument placed 1 cm apart, with each conductor tested at 5 different locations and averaged to obtain a resistivity value in Ω/cm.

Sample Preparation: The sample (1mm thick) was cut into strips of uniform size, 1 cm wide and 5 cm long for the tensile stretching test, and 1 cm wide and 10 cm long for the peeling test. The adhesive sample strip was aligned to a rigid substrate, such as plastic, with the non-adhesive end marked for grip alignment in the testing machine. The non-adhesive end was gripped securely, with the peeling angle set to 180° for the plastic substrate and 90° for the skin. The sEMG sample of CB-ecoflex electrodes was cut into a 2 × 4 cm rectangle with a thickness of 1mm.

The skin preparation procedures before electrode placement were as follows: For neutral skin, the skin was cleaned with mild soap or a degreasing agent and water to remove dirt or residues. For sweaty skin, a saline solution was used by dissolving 0.9% of NaCl in sterile water and spraying it evenly on the neutral skin surface. To oily skin to simulate sebum, a layer of Vaseline or other oil-based creams was applied to the neutral skin. To achieve optimal results, we ensured that the oil layer was thin and even.

For the washing process, the electrodes were immersed in a mild detergent solution and rubbed by hand for 1–2 min to simulate real-world washing conditions. After agitation, the electrodes were thoroughly rinsed under lukewarm running water to remove any detergent residue, then allowed to dry at room temperature. This process was repeated for a total of 50 cycles to simulate extended use.

Data Recording: sEMG signals were recorded using an electrode setup comprising Ag/AgCl and CB-ecoflex electrodes. The Ag/AgCl electrodes employed as reference electrodes were commercially available from CardinalHealth (Ireland) with trade name Kendall. The sEMG data for SNR were obtained while extending the hand to maximum position and resting periods. Data for other studies obtained from the movement/activities can be found in Figure 5.

Data Acquisition/Extraction: The sEMG signals were acquired using a commercial data acquisition system (Neuromotus TM, Integrum AB, Sweden), which was primarily developed for phantom limb pain treatment based on muscle activity recordings. In this study, we only use the Neuromotus system for sEMG acquisition. The sampling frequency was 500 Hz.

Segmentation: The sEMG signals were segmented into movements and resting periods. The segments were identified based on specific criteria, including amplitude thresholds and temporal characteristics.

The amplitude thresholds were determined by considering the characteristics of the sEMG signal. By defining appropriate window sizes and ensuring sufficient overlap, the mean amplitude within these windows was calculated.

The temporal characteristics of the segments were also taken into account. Thresholds were set to identify the boundaries of the segments. These thresholds determined the relationship between the amplitude within a window and the subsequent window, allowing for the detection of starting and ending points.

Signal Identification: Within each segmented movement, the regions of interest representing the signal were identified. These regions were defined as the intervals between a red line (the start of the contraction) and a black line (the end of the contraction). The signal segments were extracted from the sEMG data.

Noise Identification: The regions of interest representing the noise were identified based on a time shift from the black lines. Specifically, blue lines were placed 1 s (equivalent to 500 samples at a sampling frequency of 500 Hz) after each black line. The noise segments were extracted from the sEMG data between the blue lines and the subsequent red lines (or the endpoint for the last noise segment).

RMS Calculation: The RMS of the noise was calculated to quantify the magnitude of the noise. The RMS was computed by taking the square root of the mean squared amplitude of each noise segment.

SNR Calculation: The SNR was calculated as the ratio of the power of the signal to the power of the noise. The signal power was obtained by calculating the root mean squared (RMS) amplitude of the extracted signal segments. The noise power was obtained by calculating the RMS amplitude of the extracted noise segments. The SNR was expressed in decibels (dB).

Pattern Recognition: A MATLAB-based modular platform (BioPatRec) developed for hand posture recognition and finger movement discrimination in myoelectric-controlled prosthetics was used to illustrate the applicability of the CB-ecoflex electrodes.[36] Recorded sEMG signals were fed to the BioPatRec platform and the offline PatRec program was employed to evaluate the complexity of classification task. This computation can be regarded as an offline 'training', where the training algorithm can be used to discriminate between different computation options, in this study, the computation options were 'open hand' versus 'close hand' and 'flex hand' versus 'extend hand'. The output from the test is a confusion matrix telling how useful the recorded signals are in terms of discriminating between the set of hand movements.

Supporting Information

Supporting Information is available from the Wiley Online Library or from the author.

Acknowledgements

This project was primarily funded by the Swedish Knowledge Foundation (KK-stiftelsen) under the grant no. 20190110. Additionly, it recieved funding from the European Union's Horizon 2020 research and innovation programme, managed by the European Research Executive Agency (REA) under the grant agreement no. 101086071. A Marie Skłodowska-Curie Postdoctoral Research Fellowship, awarded by the European Union's Horizon Europe Programme, supported this work through the TextrodeMisc (TEXtile elecTRODE Matrix for Improved Surface eleCtromyography signal quality and usability in applications for people with limb loss) project, under the grant agreement no. 101108935. The project is also received support from China Ministry of Human Resources and Social Security Foreign Expert Program, through the International Textile Technology Innovation and Sustainability project, under the grant agreement no. G20231830001L.

Conflict of Interest

The authors declare no conflict of interest.

Author Contributions

Y.Q.W. and X.W. contributed equally to this work. Y.Q.W. and X.W. fabricated the materials, performed the material characterization tests, conducted the interfacial and electromechanical experiments, and analyzed the data. L.S. and L.G. provided the methodology (sEMG). L.G. performed the sEMG analysis. Y.Q.W., X.W., L.S., and L.G. wrote the paper. Y.Q.W. and X.W. prepared the original draft. L.S., X.Q.L., and L.G. provided conceptualization, supervision, reviewing, and editing.

Data Availability Statement

The data that support the findings of this study are available from the corresponding author upon reasonable request.

Keywords

carbon black, dry electrodes, ecoflex, skin-adhesive, surface electromyography

Received: October 10, 2024
Revised: December 20, 2024
Published online: January 22, 2025

[1] Y. Fu, J. Zhao, Y. Dong, X. Wang, *Sensors* **2020**, *20*, 3651.
[2] C. L. Ng, M. B. I. Reaz, *Measurement* **2019**, *145*, 460.
[3] M. Zhu, H. Wang, S. Li, X. Liang, M. Zhang, X. Dai, Y. Zhang, *Adv. Healthcare Mater.* **2021**, *10*, 2100646.
[4] a) L. Zhang, K. S. Kumar, H. He, C. J. Cai, X. He, H. Gao, S. Yue, C. Li, R. C.-S. Seet, H. Ren, *Nat. Commun.* **2020**, *11*, 4683; b) L. Zhang, K. S. Kumar, H. He, C. J. Cai, X. He, H. Gao, S. Yue, C. Li, R. C.-S. Seet, H. Ren, J. Ouyang, *Nat. Commun.* **2020**, *11*, 4683.

[5] J. Park, Y. Lee, T. Y. Kim, S. Hwang, J. Seo, *ACS Appl. Electron. Mater.* **2022**, *4*, 1449.
[6] a) M. M. Hossain, B. M. Li, B. Sennik, J. S. Jur, P. D. Bradford, *npj Flexible Electron.* **2022**, *6*, 97; b) H. Yuk, B. Lu, X. Zhao, *Chem. Soc. Rev.* **2019**, *48*, 1642.
[7] a) P. Zaccagnini, C. Ballin, M. Fontana, M. Parmeggiani, S. Bianco, S. Stassi, A. Pedico, S. Ferrero, A. Lamberti, *Adv. Mater. Interfaces* **2021**, *8*, 2101046; b) R. Li, K. Dong, M. Panahi-Sarmad, S. Li, X. Xiao, *ACS Appl. Electron. Mater.* **2021**, *3*, 3999; c) S. Kumar, V. Pavelyev, N. Tripathi, V. Platonov, P. Sharma, R. Ahmad, P. Mishra, A. Khosla, *J. Electrochem. Soc.* **2020**, *167*, 047506; d) M. F. Hossain, J. S. Heo, J. Nelson, I. Kim, *Information* **2019**, *10*, 325; e) T. Araki, T. Uemura, S. Yoshimoto, A. Takemoto, Y. Noda, S. Izumi, T. Sekitani, *Adv. Mater.* **2020**, *32*, 1902684; f) C.-W. Chiu, C.-Y. Huang, J.-W. Li, C.-L. Li, *ACS Appl. Mater. Interfaces* **2022**, *14*, 42441.
[8] G. Kühner, M. Voll, *Carbon Black*, Routledge, Oxfordshire **2018**, pp. 1–66.
[9] E. R. Cholleti, J. Stringer, M. Assadian, V. Battmann, C. Bowen, K. Aw, *Sensors* **2018**, *19*, 42.
[10] L. A. García-García, A. Johnson, P. M. Kreitmair, P. Lugoda, A. Pouryazdan, D. Roggen, N. Münzenrieder, *IEEE Sens. J.* **2023**, *23*, 23980.
[11] a) C. Wang, T. Yokota, T. Someya, *Chem. Rev.* **2021**, *121*, 2109; b) Z. Lou, L. Wang, K. Jiang, Z. Wei, G. Shen, *Mater. Sci. Eng.: R: Rep.* **2020**, *140*, 100523; c) Y. Yang, W. Gao, *Chem. Soc. Rev.* **2019**, *48*, 1465.
[12] P. Hubert, Y. Galerne, *Appl. Phys. Lett.* **1997**, *71*, 1050.
[13] D. E. Packham, *Int. J. Adhes. Adhes.* **2003**, *23*, 437.
[14] G. Kickelbick, *Prog. Polym. Sci.* **2003**, *28*, 83.
[15] E. Luis, H. M. Pan, A. K. Bastola, R. Bajpai, S. L. Sing, J. Song, W. Y. Yeong, *Polymers* **2020**, *12*, 2136.
[16] S. Krpovic, K. Dam-Johansen, A. L. Skov, *J. Appl. Polym. Sci.* **2021**, *138*, 50380.
[17] X. Zhao, T. Wang, Y. Li, L. Huang, S. Handschuh-Wang, *Polymers* **2019**, *11*, 948.
[18] Y. Zhang, E. Ren, H. Tang, A. Li, C. Cui, R. Guo, M. Zhou, S. Jiang, H. Shen, *J. Mater. Sci.: Mater. Electron.* **2020**, *31*, 14145.
[19] A. N. Kouediatouka, Q. Liu, F. J. Mawignon, W. Wang, J. Wang, C. Ruan, K. F. H. Yeo, G. Dong, *Appl. Surf. Sci.* **2023**, *635*, 157675.
[20] N. R. Ostyn, J. A. Steele, M. De Prins, S. P. Sree, C. V. Chandran, W. Wangermez, G. Vanbutsele, J. W. Seo, M. B. J. Roeffaers, E. Breynaert, *Nanoscale Adv.* **2019**, *1*, 2873.
[21] M. C. Biswas, S. Jeelani, V. Rangari, *Compos. Commun.* **2017**, *4*, 43.
[22] a) Z. Xu, L. Chen, L. Lu, R. Du, W. Ma, Y. Cai, X. An, H. Wu, Q. Luo, Q. Xu, Q. Zhang, X. Jia, *Adv. Funct. Mater.* **2021**, *31*, 2006432; b) X. Huang, C. Chen, X. Ma, T. Zhu, W. Ma, Q. Jin, R. Du, Y. Cai, M. Zhang, D. Kong, M. Wang, J. a. Ren, Q. Zhang, X. Jia, *Adv. Funct. Mater.* **2023**, *33*, 2302846; c) J. Cheng, J. Shang, S. Yang, J. Dou, X. Shi, X. Jiang, *Adv. Funct. Mater.* **2022**, *32*, 2200444.
[23] M. Williams, *J. Adhes.* **1972**, *4*, 307.
[24] J. Liu, S. Lin, X. Liu, Z. Qin, Y. Yang, J. Zang, X. Zhao, *Nat. Commun.* **2020**, *11*, 1071.
[25] a) Z.-M. Dang, K. Shehzad, J.-W. Zha, A. Mujahid, T. Hussain, J. Nie, C.-Y. Shi, *Compos. Sci. Technol.* **2011**, *72*, 28; b) N. T. Selvan, S. Eshwaran, A. Das, K. Stöckelhuber, S. Wießner, P. Pötschke, G. Nando, A. Chervanyov, G. Heinrich, *Sens. Actuators, A* **2016**, *239*, 102.
[26] S. M. Miriyala, Y. S. Kim, L. Liu, J. C. Grunlan, *Macromol. Chem. Phys.* **2008**, *209*, 2399.
[27] M. Sahimi, *Phys. Rep.* **1998**, *306*, 213.
[28] Y. Hu, T. Zhao, P. Zhu, Y. Zhang, X. Liang, R. Sun, C.-P. Wong, *Nano Res.* **2018**, *11*, 1938.
[29] C.-W. Nan, Y. Shen, J. Ma, *Annu. Rev. Mater. Res.* **2010**, *40*, 131.
[30] Z.-M. Dang, J.-K. Yuan, S.-H. Yao, R.-J. Liao, *Progress in Advanced Dielectrics*, World Scientific, Singapore **2020**.
[31] R. K. Mondal, K. A. Dubey, Y. K. Bhardwaj, *Polym. Compos.* **2021**, *42*, 2614.
[32] J. Li, Y. Ma, D. Huang, Z. Wang, Z. Zhang, Y. Ren, M. Hong, Y. Chen, T. Li, X. Shi, *Nano-Micro Lett.* **2022**, *14*, 132.
[33] Y. Qin, *Medical Textile Materials*, Woodhead Publishing, Cambridgeshire UK **2015**.
[34] Z. Wang, H. Wei, Y. Huang, Y. Wei, J. Chen, *Chem. Soc. Rev.* **2023**, *52*, 2992.
[35] P. Sanjuan-Alberte, M. R. Alexander, R. J. Hague, F. J. Rawson, *Bioelectron. Med.* **2018**, *4*, 1.
[36] M. Ortiz-Catalan, R. Brånemark, B. Håkansson, *Source Code Biol. Med.* **2013**, *8*, 11.